Tunable Nano-Patterns via the Constrained Dewetting of Polymer Brushes

Thomas Lee,[†] Shaun C. Hendy,[*,‡,¶] and Chiara Neto[*,†]

School of Chemistry, The University of Sydney, Sydney, NSW, 2006, Australia,
MacDiarmid Institute for Advanced Materials and Nanotechnology, Industrial Research
Ltd., Lower Hutt, 5040, New Zealand, and School of Chemical and Physical Sciences,
Victoria University of Wellington, Wellington, 6140, New Zealand

E-mail: shaun.hendy@vuw.ac.nz; chiara.neto@sydney.edu.au

Abstract

Coarse-grained molecular dynamics simulations were used to investigate the morphology and dynamics of nano-patterns formed by grafted polymer brushes on a non-adsorbing substrate as a result of constrained dewetting. As a good solvent is made to gradually evaporate, polymer brushes with low to moderate grafting density collapse into discrete nano-sized aggregates, with different types of nano-patterns possible, including pancake micelles and holey layers. The type of pattern, the size and number of features, and their dynamics depend on the grafting density of the polymer brush and amount of good solvent adsorbed. The final pattern morphology depends primarily on the total amount of material adsorbed to the surface, including both polymer and

---

[*] To whom correspondence should be addressed

[†] School of Chemistry, The University of Sydney, Sydney, NSW, 2006, Australia

[‡] MacDiarmid Institute for Advanced Materials and Nanotechnology, Industrial Research Ltd., Lower Hutt, 5040, New Zealand

[¶] School of Chemical and Physical Sciences, Victoria University of Wellington, Wellington, 6140, New Zealand

solvent. This result suggests the possibility for the use of polymer brushes as surfaces with reversibly tunable nano-patterns.

Introduction

A polymer brush, composed of polymer chains grafted by one end to a solid substrate in close arrangement, is a responsive surface capable of changing its properties in response to changes in its chemical and physical environment.[1] When exposed to a good solvent, polymer brushes become swollen. When exposed to a poor solvent, or when dried out in air, polymer brushes collapse into a compact layer. This change can be initiated by modifying the solvent composition, temperature, pH, or ionic strength,[2] or by applying an electric field.[3] Changes in the brush morphology significantly affect surface properties such as wettability, biocompatibility, corrosion resistance, and friction.[2,4,5]

While the behavior of polymer brushes under good solvent conditions has been thoroughly investigated, the poor solvent case has received less attention. Early theoretical studies made the assumption that the collapsed brush was laterally homogeneous in the plane of the surface, varying in density only with distance from the solid substrate.[6,7] More recent molecular simulations showed that this is not necessarily the case. Depending on the grafting density of the brush and the wettability of the polymer on the substrate, the polymers may collapse and aggregate such that some regions of the substrate become exposed.[8–11] Such a situation arises when the favorable decrease in surface energy resulting from the dewetting is greater than the increase in free energy that results from unfavorable stretched conformations of some of the polymer chains.[8] This phenomenon has been given the name “constrained dewetting”.

A variety of different nano-patterns may be formed on the surface as a result of constrained dewetting, representative example of which can be seen in Figure 1, which shows how the patterns change with grafting density (more detail later in the results section).

Much of the understanding of the nature of these patterns has been obtained using molecular simulations. Such studies have identified several pattern morphology regimes, including pinned micelles (also known as octopus micelles),[10,11] pancake micelles,[8] worm-like layers (also known as striped or lamella layers),[9,10] and holey layers.[8,9]

Experimental studies employing atomic force microscopy have confirmed the formation of these patterns,[12–15] and there have been attempts to model these systems using self-consistent field methods.[9,16] Theoretical models were developed early on to describe the low grafting density pinned micelle regime,[7,17] but the patterns at higher grafting densities depend on a multitude of factors and resist a simple description. Huh et al.[8] derived non-linear expressions for the free energy of the pancake micelle and holey layer patterns, and predicted feature size and density as a function of grafting density and chain length.

To the best of our knowledge, there has been no study of how the patterns resulting from constrained dewetting are influenced by the presence of a small amount of good solvent – less than that required to completely swell and homogenize the grafted polymer layer. In this work we have used coarse-grained molecular dynamics simulations to demonstrate that the morphology of the patterns formed by the brushes can be dynamically tuned by adsorbing a small amount of good solvent into the layer. A polymer brush, covered by a thin layer of an explicitly modelled good solvent, was subjected to the evaporation of the solvent, which caused constrained dewetting. The nano-patterns formed as the evaporation proceeded evolved from a homogeneous layer to discrete micelles with numerous intermediate aggregate morphologies. The features of the pattern depend strongly on the amount of solvent adsorbed to the layer and the grafting density. For the first time, we have characterized the dependence of the dynamics of these patterns as a function of grafting density and solvent content. We propose that, by controlling the solvent adsorption, grafted polymer layers could be used as reversibly tunable nano-patterned surfaces, for example as switchable mixed-boundary-condition surfaces with potential application in microfluidic devices.[18]

Methodology

Coarse-grained molecular dynamics simulations were run using the free open-source LAMMPS molecular dynamics package.[19] The 3-dimensional simulation contained four types of particles: monomer, solvent, substrate, and anchor – an immobile, non-interacting particle in the plane of the substrate to which the first monomer of the polymer chain was bound.

Any two non-bonded particles in the system separated by a distance r interacted via a Lennard-Jones potential:

$$U_{i,j} = 4\epsilon_{\mathrm{i,j}} \left[\left(\frac{\sigma}{r} \right)^{12} - \left(\frac{\sigma}{r} \right)^{6} \right] \; ; \; r < r_c \tag{1}$$

where $\epsilon_{i,j}$ determines the strength of the interaction between two particles i and j; σ is approximately the range of the repulsive part of the potential, the effective size of the particles; and r_{c} is the force cutoff distance, set to 2.5σ. All length scales are referred to in terms of σ, which in the simulations was set to one for all particles. The σ parameter corresponds to the monomer size, which is on the order of angstroms for common polymers, for example the approximate monomer lengths of polystyrene, polyethylene oxide, and polyvinyl alcohol are 4.0 Å,[20] 2.8 Å,[21] and 2.5 Å[22] respectively (determined from x-ray scattering studies of the crystalline polymers). The parameter $\epsilon_{i,j}$ depends on the nature of the interacting particles. Energies are referred to in units of $\epsilon = \epsilon_{\mathrm{solvent,solvent}}$. For interactions between any like particles, $\epsilon_{\mathrm{like}} = 1\epsilon$. For the solvent-polymer interaction $\epsilon_{\mathrm{solvent,polymer}} = 1\epsilon$, making the solvent an athermal solvent for the polymer. Interactions between solvent and substrate or monomer and substrate particles $\epsilon_{\mathrm{i,substrate}} = 0.5\epsilon$, such that the substrate was relatively non-wetting. The substrate was composed of immobile particles arranged in a square array with period 1σ lying in the xy plane. We chose a square array rather than a random grafting pattern due to concerns that the latter option would require the simulated surface to be much larger in order to sample a statistically significant area. Several studies have provided evidence that the polymer aggregates arrange in a hexagonal pattern on the surface regardless of the underlying pattern of graft points.[8–10]

The covalent bonds between the monomer particles which make up the polymer were simulated by a spring-like interaction described by a finitely extensible nonlinear elastic (FENE) potential:[23]

$$U_{i,j} = -0.5KR_0^2 \ln\left[1 - \left(\frac{r}{R_0}\right)\right] + 4\epsilon\left[\left(\frac{\sigma}{r}\right)^{12} - \left(\frac{\sigma}{r}\right)^{6}\right] + \epsilon \qquad (2)$$

where the first term cuts off at R_0 and the second at r_c. Typical values for the parameters were $K = 30\epsilon/\sigma^2$ and $R_0 = 1.5\sigma$. Polymers were grafted in a square array on the surface with period $\rho^{-1/2}$ where ρ is the grafting density. Each polymer contained 24 monomer particles.

The equations of motion for the solvent and polymer particles were integrated using a velocity-Verlet algorithm with a time-step of 0.01τ, where $\tau = (m\sigma^2/\epsilon)$ is the Lennard-Jones time unit, and m is the mass of a particle. A Langevin thermostat[24] was applied to the polymer and solvent particles. This maintains a constant temperature by the addition to each particle of a dissipative force given by $\mathbf{F}^\mathrm{d} = -\gamma\mathbf{v}$, and a random force with magnitude proportional to $\sqrt{\gamma T/dt}$, where γ is the friction coefficient, T is the temperature, set to 1, and dt is the timestep. The friction coefficient was $0.2\tau^{-1}$ while collecting data on equilibrium state, and $5\tau^{-1}$ during equilibration and evaporation to speed up the equilibration of polymer morphology and solvent adsorption.

The simulation box was 25σ long in the z dimension – perpendicular to the substrate – and between 75σ and 90σ in the x and y dimensions, depending on the grafing density. The variation in size was required in order to match the period of the graft-points with the box dimensions. Periodic boundary conditions were applied in the x and y directions. Any particles crossing the upper z boundary of the simulation were reflected back into the simulation box.

In the evaporation simulations, between 2 and 4 solvent atoms for every σ^2 of substrate area were introduced at the start of the simulation, the exact number depending on the polymer grafting density. More solvent atoms were required at the start of the low grafting density simulations in order to ensure the initial state corresponded to a swollen homogeneous layers. Evaporation of the solvent was achieved by removing two solvent particles every 20τ from the upper region within 5σ from the top of the simulation box, in order to avoid disturbing the polymer during the removal. This corresponds approximately to an evaporation rate on the order of 1-5 mm/s for typical solvents. The end-points of these evaporations were used for the study of the polymer brushes in the complete absence of solvent in the sections titled “Morphology in the absence of good solvent” and “Quantitative analysis of morphology”.

Method for morphology analysis

Pattern characteristics were quantified using a component-labeling region detection method to identify and analyze continuous regions of polymer-covered surface and bare substrate. Polymer covered regions completely enclosed by bare substrate are referred to as “islands”, while regions of bare substrate entirely enclosed by polymer as “holes”. The method can be applied to surface density images such as those shown in Figure 1, in which the shade of each point corresponds to the number of particles in a $1\sigma \times 1\sigma$ region of the surface. A noise reducing filter is applied to the image prior to analysis which sets the density of every point to the average density of the $3\sigma \times 3\sigma$ square region centered on that point.

The method requires a minimum surface density threshold to be specified to determine the cut-off between covered and uncovered regions of the surface, as well as a minimum feature area threshold corresponding to the the minimum size of the features of interest. The surface density threshold was $0.5\sigma^{-2}$ and the minimum feature area $15\sigma^2$. We then obtain a binary image from the surface density data using the threshold surface density, such that any data point with a value less than the threshold becomes a black pixel, and all others become white pixels; it then identifies all continuous regions of black pixels and all regions of white pixels, based on a component-labeling region detection algorithm.[25] Finally we compute the number of islands, number of holes, and mean and standard deviation of island and hole size in pixels. More details on the method are provided in the Supporting Information.

Results and discussion

We will first consider the equilibrium morphologies of the polymer layer in the absence of solvent. This will be followed by our analysis of the effects of adsorbed solvent on the patterns and the distribution of the solvent on the surface. We will then consider how the pattern features dynamically change over time.

Morphology in the absence of good solvent

Firstly, the collapse of grafted polymer layers was examined in the absence of any solvent, and our results compared with previous computational and theoretical studies. We comment on some features of the patterns that appear to have been neglected by earlier studies, including the linearity of surface coverage with grafting density, and the formation of conjoined holes and micelles near the worm-like layer regime.

Examples of the patterns formed as a result of the constrained dewetting of the brushes are shown in Figure 1, which illustrates the distribution of monomers across the surface at gradually increasing grafting densities (parts A – G). These images are representative snapshots taken from the simulations. The solvent-free surfaces were prepared by starting with a swollen brush and performing an evaporation simulation, as described in the Methodology section above. The end-points of the evaporations were allowed to equilibrate for at least 40000τ after the last of the solvent was removed. This method allowed the pattern to slowly progress towards the final state via intermediate states in which the polymer chains mobility was higher due to the presence of the solvent, reducing the opportunity for the surfaces to

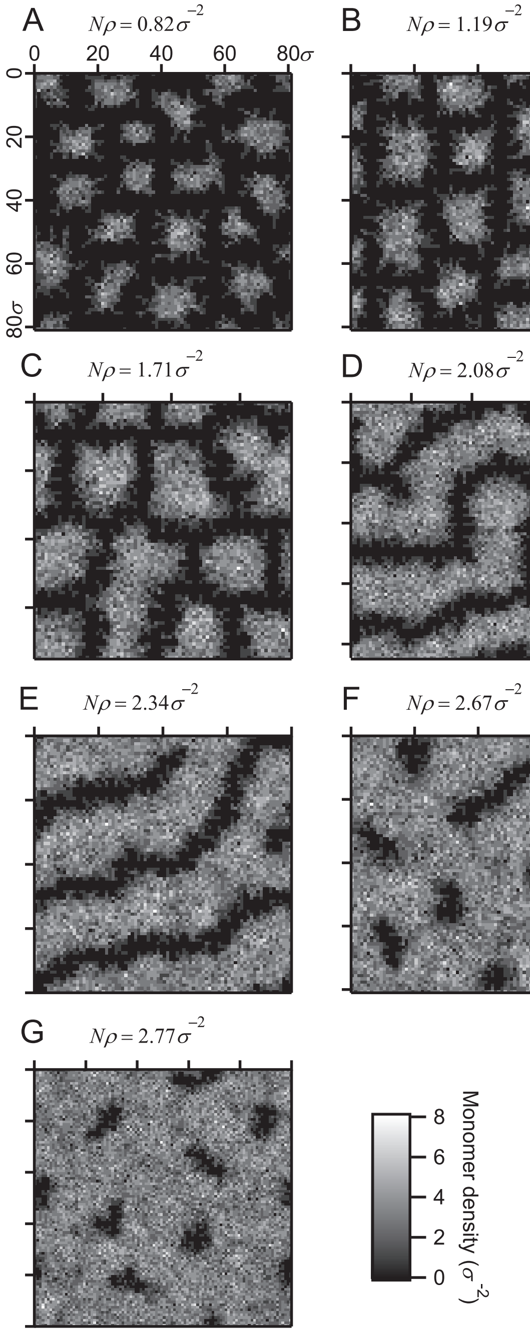

Figure 1: Typical snapshots of the distribution of polymer across the surface resulting from the collapse of a polymer brush in the absence of solvent, in order of increasing polymer grafting density (number of chains per unit area ρ multiplied by the chain length N, equivalent to the mean number of monomers per unit area). The morphologies are identified as: A pinned micelles; B and C pancake micelles; D and E worm-like micelles; F and G holey layer. Each pixel represents the number of monomers over a $1\sigma \times 1\sigma$ square region of the surface at a particular point in time.

become kinetically trapped in local free-energy minima far from the thermodynamic equilibrium arrangement. As always with molecular dynamics simulations, it is very difficult be certain that the simulated system is at thermodynamic equilibrium. The possibility remains that we may be observing a kinetically trapped state and this may be why some of these structures (the worm-like features and holey layers described below) have not been observed experimentally.

At low grafting density, Figure 1A, pinned micelles form. These structures form by the grouping of several nearby polymer chains to form a central nucleus. While some chains have their graft-points located directly under this nucleus, a significant number stretch out over the uncovered surface in order to join the nucleus. The region around the nucleus in which the tethers are located is referred to as the corona. If we take the unit of distance σ to be on the order of several angstroms, then the micelle diameter would be approximately on the order of 10 nm. Previous simulation studies have noted that the nuclei appear to favor a hexagonal arrangement on the surface.[8,9] Theoretical studies by Huh et al. suggest that the hexagonal arrangement is the most thermodynamically favorable.[8] Pinned micelles have been observed in physical experiments using atomic force microscopy (AFM).[12,13]

As grafting density is increased, Figures 1B and C, the size of the micelles increases accordingly. The corona region shrinks, as the chains do not need to stretch as far to reach the nucleus. These larger aggregates have more flattened aspect ratios, up to approximately 4:1 width:height in our simulations, relative to the pinned micelles in Figure 1A. Due to their characteristic shape, these features were dubbed by Huh et al.[8] “pancake micelles”.

At the higher grafting density end of the pancake micelle regime it is not uncommon to observe elongated aggregates, as seen in Figure 1C, which appear to form as a result of the fusion of two neighboring pancake micelles. Such conjoined structures have also been observed by AFM[12,13] and in other simulations.[9] As grafting density is increased further, the number of connections between micelles increases until worm-like features emerge, seen in Figures 1D and E, which in part E extend across the entire length of the simulation box.

Worm-like aggregates are less commonly reported in the literature.[9,10] A scaling analysis by Pattanayek et al.[9] suggests that this arrangement provides the best compromise between tether and surface energy within a narrow range of grafting densities between the holey and pinned micelle layer. A more detail analysis by Huh et al.,[8] which makes fewer assumptions about the tether length relative to the nucleus size, reported that the worm-like layer is never the most stable. To our knowledge they have not yet been observed experimentally.

At still higher grafting densities the holey layer regime is reached, characterized by small regions of exposed substrate surrounded by polymer, as seen in Figures 1F and G. Polymer chains with tether points within the hole must stretch towards the boundary. At the lower grafting density end of this regime elongated holes are observed, while at the higher end the holes are roughly symmetric. There is a critical grafting density, above which the homogeneous layer is stable and no constrained dewetting occurs, which is quantified in the next section. To our knowledge the holey layer has not been observed in physical experiments, but have been predicted by both Monte Carlo simulations and self-consistent field calculations, and an analysis of the free energy contributions of the surface and tethering energies suggests that there is a range in which the holey layer is more stable than the pinned micelle configuration and homogeneous layer.[8,9] The appearance of non-circular holes is in agreement with the calculations by Huh et al.[8] which show larger holes can reduce their free energy by allowing "crinkling" of the perimeter in order to reduce the stretching length of the tethers within the hole.

Quantitative analysis of morphology

The average characteristics of the collapsed polymer layer were analyzed over time, including coverage area, average radius of gyration, and the number and size of the pattern features. As will be discussed in detail later in this article, the pattern features of some surfaces were observed to fluctuate over the course of the simulation. In order to ensure an equilibrium was reached, pattern characteristics were monitored over a period of 40000τ to 80000τ. If significant drift was observed the simulation was restarted and allowed to run for a further 40000τ before again repeating the test for equilibrium. Except where otherwise specified, average values are obtained from a set of snapshots of the simulation taken every 400τ over a period of 40000τ to 80000τ. The error bars shown in the figures are the standard deviation of the set of values collected over all the snapshots unless otherwise stated.

In Figure 2A the fraction of the surface covered by polymer, A, is plotted as a function of grafting density, expressed as $N\rho$. The surface coverage fraction is calculated from two-dimensional snapshots like those shown in Figure 1. The surface coverage fraction A is the fraction of pixels with a monomer density greater than zero. The coverage increases with grafting density, and appears to do so approximately linearly, unperturbed by the transition between different pattern regimes.

The gradient of the linear fit, with units of σ^2/monomer, represents the amount of area covered per monomer. The variation in A between snapshots is small, with standard deviations less than 1%. Huh et al. predicted that there is a critical value of grafting density ρ_c above which a homogeneous layer is always formed, given by:

$$\rho_c = \sqrt{6}/(4\sqrt{N}a^2) \tag{3}$$

where a is the monomer size.[8] For our system the critical grafting density is predicted to be exactly $N\rho_c = 3\sigma^{-2}$. Extrapolating the linear fit in Figure 2A gives a result $N\rho_c = (3.03 \pm 0.16)\sigma^{-2}$, consistent with the prediction.

The linearity in coverage area is a consequence of the fact that the density and height of the polymer aggregates is approximately constant, and that the polymer aggregates are relatively flat. The height was measured in terms of the average z-component of the radius of gyration R_{gz}, shown as a function of grafting density in Figure 2B. In the intermediate grafting density range where holey layers, worm-like layers, and pancake micelles are present, R_{gz} varies by as little as 5% between different grafting densities. It drops more significantly

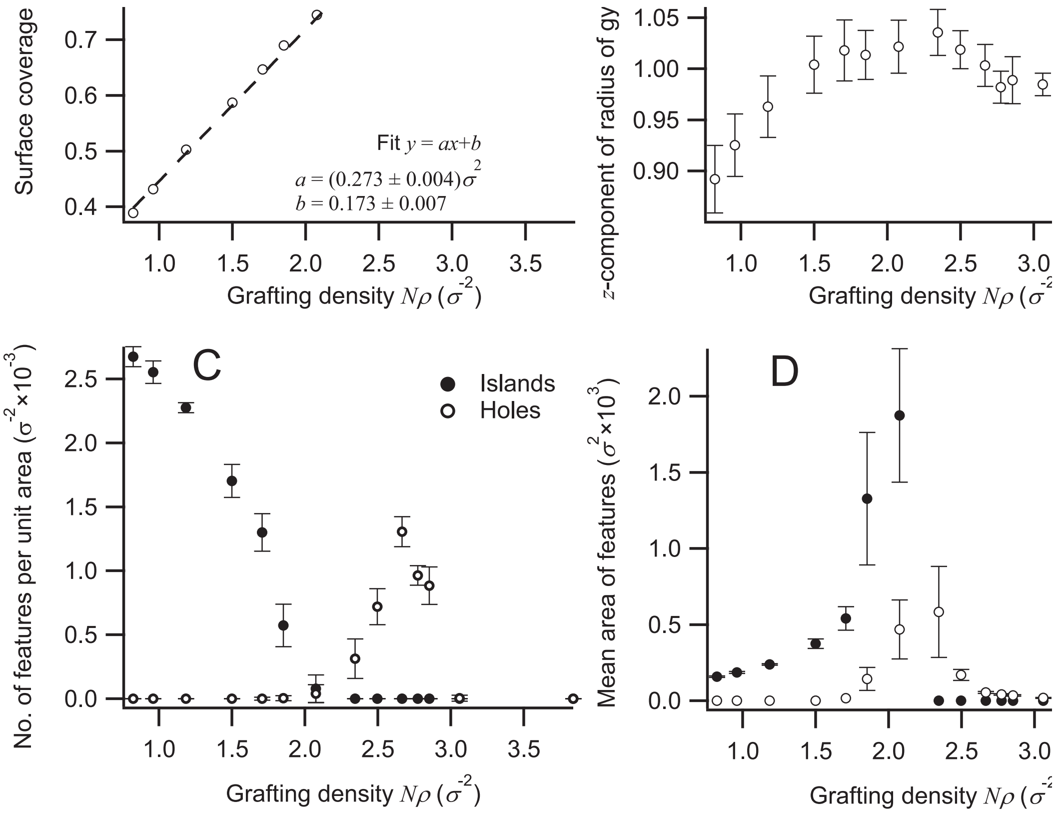

Figure 2: Changes in the characteristics of the patterns formed by polymer brushes in the absence of a solvent as a function of grafting density, expressed as the number of monomers per unit area $N\rho$, where $N = 24$. A – fraction of the surface covered by polymer; B – the mean z-component of the radius of gyration; C – the number of discrete polymer aggregates ("islands", filled circles) and discrete regions of bare surface surrounded by polymer ("holes", empty circles) per unit area; and D – the average size of the islands and holes (same symbols as in C). The standard deviations in A are slightly smaller than size of the markers, and in B, C and D are represented by the error bars. The dashed line in A indicates a linear fit to the data, excluding points where a homogeneous layer was formed. The gradient and y-axis intercept of the fits are given in the figure.

at low grafting density, in the pinned micelle regime, due to the fact that a greater proportion of the monomers are in the corona rather than the nucleus. But even this drop is relatively small, at a mere 0.1σ less than R_{gz} in the pancake micelle regime. These trends are consistent with earlier measurements by Huh et al..[8]

Figure 2C illustrates the average number of discrete polymer islands and number of holes per unit area as a function of grafting density, and in Figure 2D their average size is plotted. A time-averaged area was calculated by first calculating the average island area for each snapshot, then averaging the results from all snapshots.

Islands and holes are not observed to coexist in significant numbers at any given grafting density. At low grafting densities, as seen in Figures 1A, B and C, islands clearly dominate. As grafting density increases, the number of islands decreases and the average island area increases, until a point is reached, close to $N\rho = 2\sigma^{-2}$, at which no discrete isolated polymer covered regions remain. At higher grafting densities, the polymer is arranged either into worm-like aggregates seen in Figures 1D and E, or a continuous background phase as seen in Figures 1F and G. The rapid increase in island area as the number of islands approaches zero, seen in Figure 2D, occurs because the size and density of micelles forces the fusion of neighbors into larger features. The large standard deviation of the average island area in this region indicate that these fusion events result in islands with a wide variety of sizes. The dynamics of these fusion events are described in detail later in this article.

As grafting density is increased further, the first discrete holes appear somewhere in the range $2.0\sigma^{-2} < N\rho < 2.3\sigma^{-2}$. As the grafting density increases both the number and size of the holes first increases, then decreases until a continuous layer is formed at a point near $3.0\sigma^{-2}$. When these holes first appear they have the elongated appearance seen in Figure 1F, as if multiple smaller holes have fused together. As for the micelle case, the dynamics of the formation of these features is described later. As grafting density increases, smaller more symmetric holes become dominant, as seen in Figure 1G.

Morphology as a function of adsorbed solvent

The effect of the amount of a good solvent adsorbed to the polymer brush was investigated. The model solvent was composed of free monomers – that is, Lennard-Jones particles with interaction potentials identical to those of the monomers but without any bonding potential. At various grafting densities, the system was initialized with a large number of solvent atoms, such that the polymer brush formed a homogeneous layer. After equilibration the solvent was slowly removed until none remained. Snapshots of the system were recorded at intervals throughout the solvent removal process. Animations of the changes in polymer density across the surface are provided in the Supporting Information.

An analogous physical experiment might be performed by exposing a brush to a vapor of good (and athermal) solvent at various pressures, or by immersing a brush in a binary solvent mixture in which the majority component is a very poor solvent and the minority component a good solvent, and varying the concentration of the good solvent component. In either case, good solvent is preferentially adsorbed into the polymer layer such that an excess is present near the substrate. In our simulation the solvent – like the polymer – did not wet the underlying substrate, with the Lennard-Jones energy parameter $\epsilon_{\mathrm{solvent,substrate}} = 0.5\epsilon_{\mathrm{solvent,solvent}}$, and so did not adsorb strongly to exposed regions of the substrate.

As described earlier with regard to the surfaces in the absence of solvent, there is a critical grafting density ρ_c which is the maximum grafting density at which a continuous polymer layer is formed with no constrained dewetting. In the evaporation simulations, if $\rho < \rho_c$ then at some point during the solvent removal process constrained dewetting must occur. Adsorption of solvent tended to change the morphology of the layer in such a way that it resembled a layer with higher grafting density. As solvent was removed from a brush with $N\rho = 2.34\sigma^{-2}$, for which the corresponding solvent-free surface is shown in Figure 1E, the brush initially formed a small number of holes, which increased in number as more solvent was removed, eventually joining together to form elongated holes, and then the final worm-like features. Lower grafting density brushes, which formed pinned micelles in the absence of solvent, did not show a clear holey layer, but formed worm-like features and then larger pancake micelles before shrinking into their solvent-free state.

Dynamically removing solvent from the system over the course of the simulation is a convenient way to observe the full spectrum of morphologies possible for different amounts of adsorbed solvent. However, there is a risk that the morphology at any given point in time could be dependent on the solvent removal rate if this rate is not slow enough to allow the system to fully relaxed into an equilibrium state. It is also difficult to quantitatively characterize the pattern due to the relatively small number of data points at each value of surface excess. To overcome these issues, the equilibrium behavior of a brush with a given amount of adsorbed solvent was analyzed by saving the simulation state at regular intervals during the solvent removal, starting new simulations from the saved states. These restarted simulations were then analyzed in the same manner as the solvent free surfaces, with the morphology of the layer at equilibrium being averaged over a period of between 40000τ and 80000τ.

Relationship between morphology and solvent excess

The dependence of pattern morphology on the amount of solvent adsorbed to the brush was quantified. The adsorption was characterized by the surface excess concentration Γ_s – defined as the amount of material per unit area present on the surface in excess of the amount that would be expected if the concentration at the surface was the same as that in the bulk.[26] The bulk solvent density Φ_bulk was measured in the simulations by first measuring the density of solvent far from the brush over time in a range of z in which the solvent density was constant. The bulk solvent density was subtracted from the time-averaged monomer density-versus-z profile, resulting in a profile of the excess solvent density. The solvent surface excess Γ_s was calculated by integrating the positive regions of the excess solvent density profile i.e. those regions in which the solvent was in excess compared to the bulk.

We have found that a key parameter on which the morphology of the polymer brushes

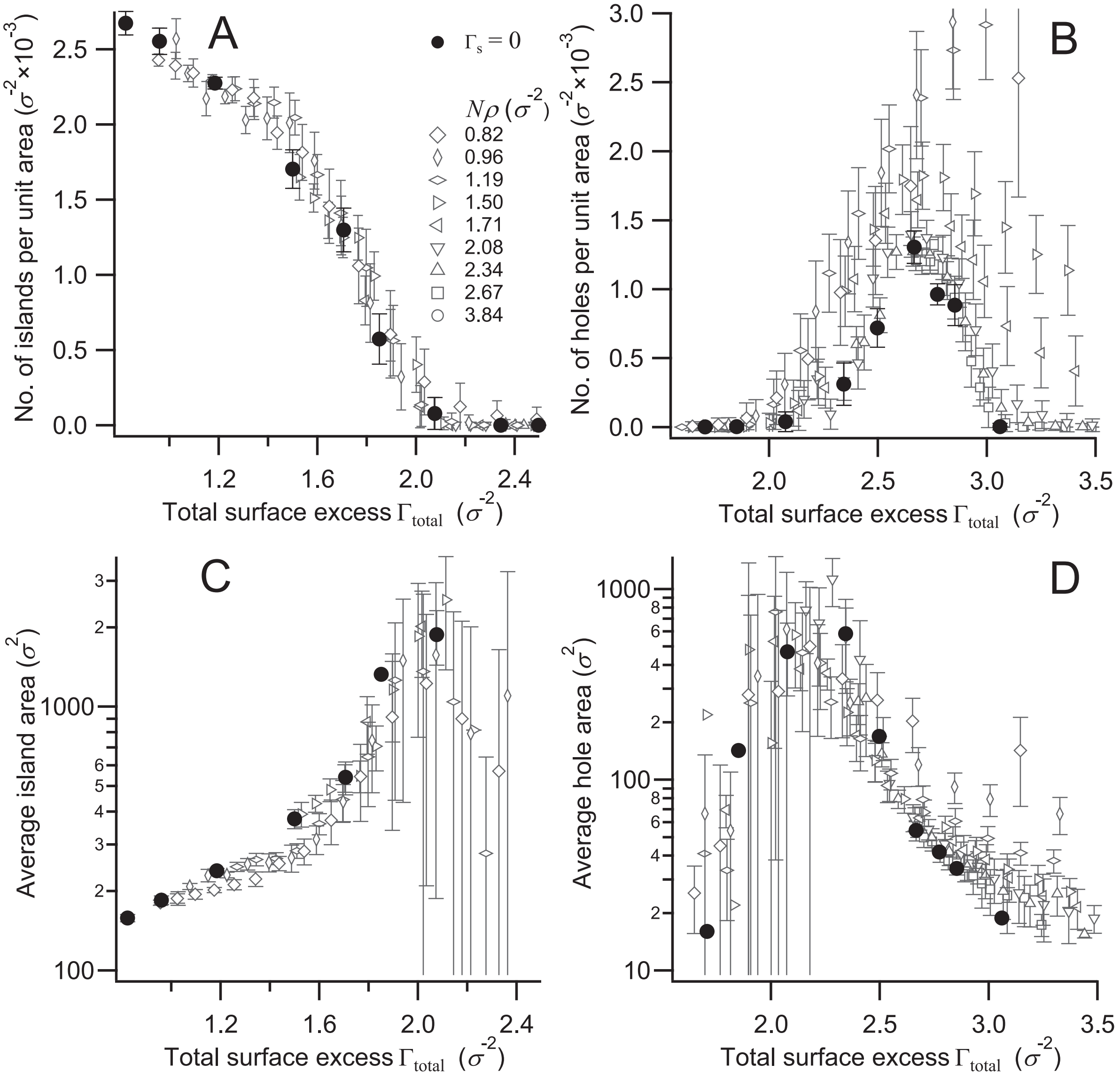

Figure 3: Number of islands (A) and holes (B) per unit area and their mean area, respectively C and D, plotted on a log scale, for different grafting densities as a function of the total surface excess $\Gamma_{\text{total}} = \Gamma_s + N\rho$, which is the total number of monomers and adsorbed solvent per unit area. This is *not* the same quantity as used for the horizontal axis in Figure 2, which used the number of monomers $N\rho$ only. The results for the solvent free surfaces ($\Gamma_s = 0$) are shown as filled circles. The data points represent the mean value averaged over all the snapshots taken during the simulation, and the error bars indicate the standard deviation.

depends is the sum of the number of monomer per unit area and the surfaces excess concentration of solvent $N\rho + \Gamma_{\mathrm{s}}$ i.e. the total number of particles per unit area at the surface, including both monomers and solvent particles. We will use the term “total surface excess”, denoted Γ_{total}, to refer to this parameter, with the reasoning that it is effectively the sum of the surface excesses of monomer and solvent particles. It follows from the definition that two surfaces with the same total surface excess may have both different grafting density and solvent content.

In Figure 3A and B the number of islands and holes are plotted respectively as a function of the total surface excess Γ_{total}. Each different shaped open symbol corresponds to a different grafting density. Because the $N\rho$ component of the total surface excess is constant for a given grafting density, moving along the horizontal axis represents a change in the solvent surface excess component Γ_{s}. The filled circles on the plot represent the results for the solvent-free surfaces. When plotted in this way, a remarkable degree of overlap between the different grafting densities studied can be seen. Looking first at the number of islands per unit area in Figure 3A, the number of islands present for a given Γ_{total} depends very little on the grafting density of the brush. In all cases the value of Γ_{total} at which islands are no longer present in significant numbers is close to $2.2\sigma^{-2}$ – marking the transition point between pancake micelle and worm-like layer regimes.

The size of the islands, plotted in Figure 3C, is also very similar between the different grafting densities, increasing with the total surface excess. The standard deviation of the island size also increases with Γ_{total}, particularly when $\Gamma_{\mathrm{total}} > 1.6\sigma^{-2}$ due to the joining of neighboring micelles resulting in a greater distribution of micelle sizes as the worm-like regime is approached, as was noted earlier for the solvent-free surfaces.

The number of holes per unit area, shown in Figure 3B, is not as consistent between grafting densities as it is for the islands. The data points for high grafting density brushes in Figure 3B for which $N\rho > 2.08\sigma$, agree reasonably well with each other and with the dry layer results. At grafting densities $N\rho < 2.08\sigma$, the number of holes per unit area is greater than that observed in the dry layer at the same Γ_{total}. This is due largely to the fact that this data is calculated based purely on the polymer positions without taking into account the location of the solvent. We will show later in this article that when the excess solvent is included, the agreement between grafting densities is much improved. Regardless of grafting density, discrete holes are not stable in the range $\Gamma_{\text{total}} < 2.0\sigma^{-2}$, which, as already seen, is micelle-dominated.

The average hole size is shown in Figure 3D on a log scale to capture the wide range of possible length scales. The trends here mirror those described for the micelles, although the agreement between grafting densities is not as good. In the range $2.3\sigma^{-2} < \Gamma_{\text{total}} < 3.0\sigma^{-2}$ the hole size increases as surface excess decreases, except for the lower grafting density surfaces, for which the behavior is less well defined. The distribution of sizes, indicated by the standard deviation, is relatively tight. When Γ_{total} falls below $2.5\sigma^{-2}$, the size continues to increase, but the standard deviation increases significantly, indicating that a wide distribution of hole sizes are present due to the fusion of nearby holes.

Location of the solvent

Solvent was found to be in excess in the regions occupied by the polymer, as expected due to the solvophobic nature of the substrate and solvophilic nature of the polymer. An example for a particular surface is illustrated in Figure 4A, in which the surface density of the polymer is shown, and in Figure 4B where the surface excess of the solvent across the surface is shown. The latter is obtained by measuring the number of solvent atoms above each $1\sigma \times 1\sigma$ region of the surface, then subtracting the number of solvent atoms expected to be present if the solvent atom density in that volume was equal to the bulk density Φ_{bulk}. As the resulting image is very noisy, an averaging filter has been applied, which renormalizes the value of each pixel to the mean of its original value and that of its 8 nearest neighbours. By comparing Figures 4A and B, it is clear that the solvent surface excess is higher at the locations where the polymer micelles are present, i.e. the polymer and solvent are co-localized.

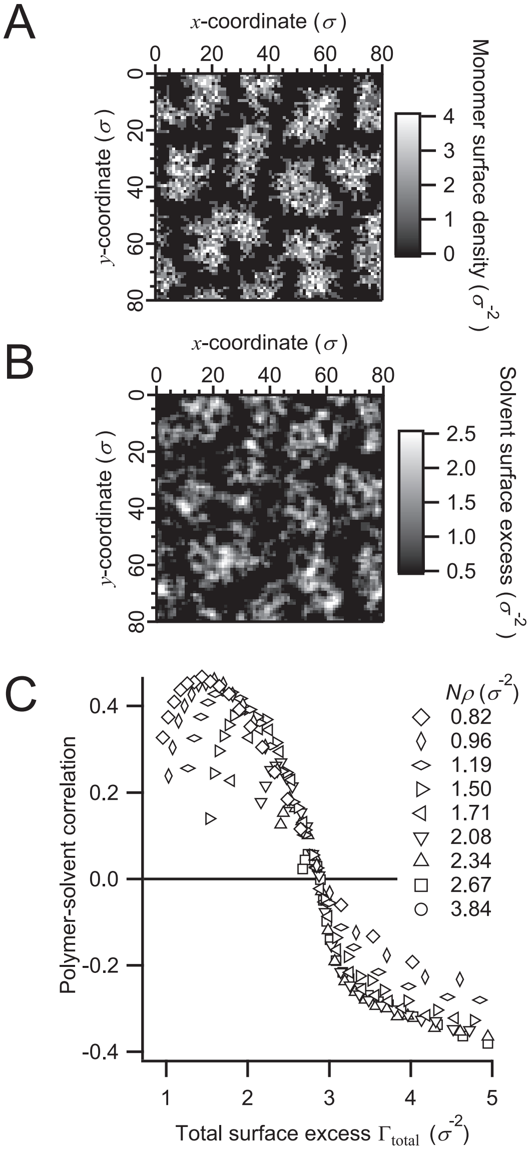

Figure 4: (A) Snapshot of the polymer surface density at a particular point in time for a brush surface with $N = 24$, $N\rho = 0.96\sigma^{-2}$ and $\Gamma_{\text{total}} = 1.7\sigma^{-2}$. (B) Solvent surface excess for the same surface as A, with the contrast adjusted so that all pixels with a value less than $0.5\sigma^{-2}$ appear black and all with a value greater than $2\sigma^{-2}$ are white, in order to improve clarity. (C) Degree of linear correlation between solvent and polymer surface excess for the different grafting densities as a function of total surface excess in terms of the Pearson's correlation coefficient (Equation 4).

The correlation between solvent and polymer is a general feature of this system, as demonstrated by evaluation of Pearson's correlation coefficient, which is plotted in Figure 4C for the various grafting densities as a function of Γ_{total}. The Pearson's correlation coefficient for two samples of variables P and S (which need not necessarily correspond to two images), with n samples each and sample standard deviations s_P and s_S respectively is defined as:

$$r = \frac{1}{n-1} \sum_{i=1}^{n} \left(\frac{P_i - \bar{P}}{s_P} \right) \left(\frac{S_i - \bar{S}}{s_S} \right) \tag{4}$$

In our case each value i corresponds to a particular pixel, with P_i being the polymer surface concentration at the ith pixel and S_i being the solvent surface excess at that same pixel. The coefficient is a measure of linearity, in our case a test of the degree to which the solvent surface excess varies linearly with the monomer density. The coefficient must have a value between $+1$ and -1, where $+1$ indicates perfect linear correlation, -1 indicates perfect anti-correlation, and 0 indicates no correlation.

Figure 4C demonstrates that the polymer and solvent have a positive correlation when $\Gamma_{\text{total}} < 3\sigma^{-2}$, which unambiguously indicates that the solvent adsorbed preferentially to the polymer. In the homogeneous layer regime, where $\Gamma_{\text{total}} > 3\sigma^{-2}$, the correlation coefficient is negative. This indicates anti-correlation between the polymer and solvent. This is due to the fact that at any given moment in time, the polymer and solvent cannot occupy the same region (due to the strong short-range repulsion between them). Any region of the surface that happens to be deficient of polymer due to random movements of the polymer chains will tend to contain additional solvent to fill the void left by the polymer. In this case the length scale of the anti-correlation is much less than that of the correlation observed in the systems which undergo constrained dewetting.

Performing a pattern analysis on combined density images in which both polymer and excess solvent were accounted for (see Supporting Information for details), helped in understanding the solvent-free case.

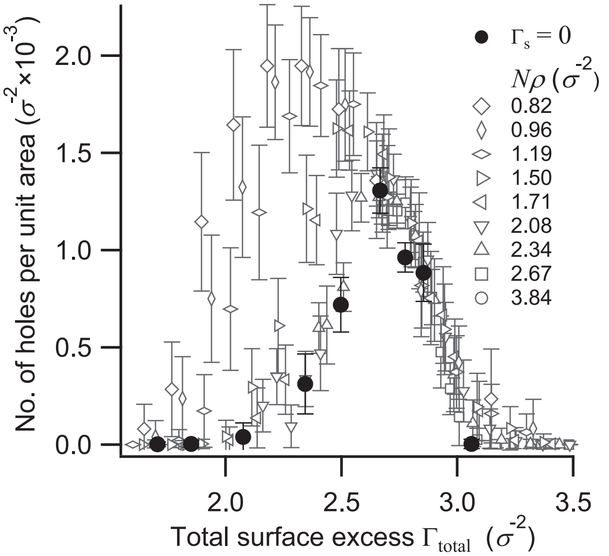

Figure 5: The number of holes per unit area as a function of the total surface excess, measured in the same manner as the data in Figure 3B, but taking into account the location of excess solvent on the surface, allowing true gaps in the polymer coverage to be separated from solvent-filled polymer deficient regions.

Comparing the results in Figure 5, in which both adsorbed solvent and polymer are included, with Figure 3B, in which only the polymer is included, a significant difference in the number of holes at low grafting density can be observed. There is now much better agreement between the number of holes per unit area at different grafting densities in the range $\Gamma_s + N\rho > 2.6\sigma^{-2}$, whereas in Figure 3B far more holes were observed at low grafting density in this same range of Γ_{total}. This new agreement suggests that many of the holes identified when only the monomer positions were accounted for were only temporary fluctuations in polymer density, and were in fact filled with solvent.

In the region $2.0\sigma^{-2} < \Gamma_{\mathrm{total}} < 2.6\sigma^{-2}$, the regime of conjoined holes and worm-like aggregates, there is less agreement between grafting densities in Figure 5 compared to when only the polymer was taken into account in Figure 3B. In addition, when solvent is included, holes persist at lower values of Γ_{total}, extending into what appears in Figure 3 to be the micelle regime. Visual inspection of the images suggests that this effect is the result of solvent atoms forming connections between polymer aggregates. The interconnections between micelles create the appearance of a holey layer, even though the polymer itself forms discrete aggregates. This also accounts for the large standard deviation in the number of holes and islands at low grafting densities in the range approximately corresponding to $1.3\sigma^{-2} < \Gamma_{\mathrm{total}} < 2.6\sigma^{-2}$, seen in Figures 3A and B.

Dynamics of collapsed brushes

In many of our simulations the nano-patterns formed by constrained dewetting fluctuated significantly over time. These dynamic properties were investigated by measuring the frequency with which the numbers of islands and holes in the pattern changed. To our knowledge there have been no previous studies of the changes over time in these patterns. As a coarse-grained polymer model is employed in these simulations, we aim to make qualitative observations regarding the types of changes the patterns undergo, and the relative frequency with which these changes occur at different values of grafting density and solvent content.

Figure 6 illustrates how variations in the grafting density and surface excess contribute to the frequency with which the number of holes and islands changes. The frequency is calculated as the sum of the magnitude of every change in the number density of holes or islands between successive snapshots throughout the simulation, divided by the total duration. Because the simulation state is only sampled every 400τ, it is possible that the frequency is underestimated, particularly in the more dynamic layers. It is also possible that some changes are missed when two changes occur between snapshots that cancel each other out. These limitations should not prevent us from making comparisons between the systems at different grafting densities and surface excesses.

In Figure 6A we see that as the grafting density increases, the frequency of morphological changes is relatively low but gradually increasing in the range $\Gamma_{\mathrm{total}} < 1.5\sigma^{-2}$. In this regime the pinned micelles are separated by significant distances and polymer chains tend to be trapped in a particular micelle. As the total surface excess increases into the pancake micelle regime, the frequency of changes increases significantly. Two processes are possible which

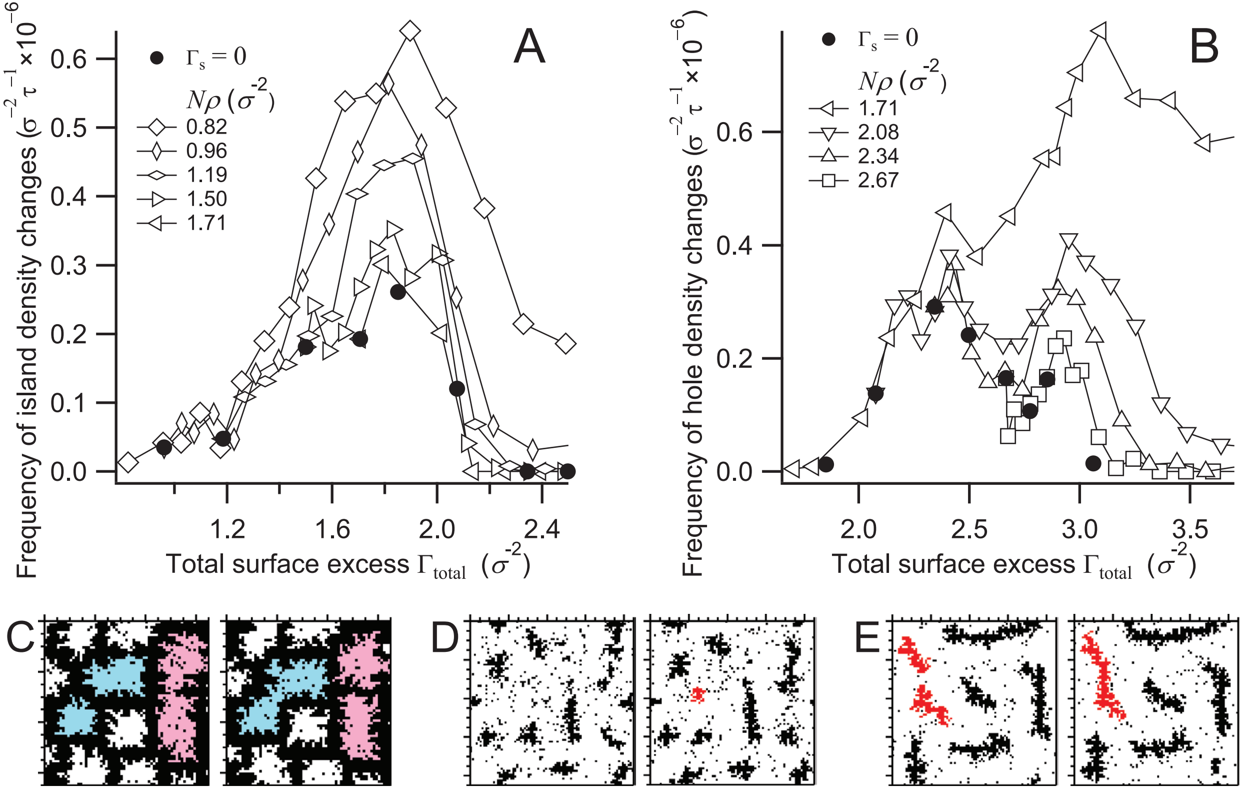

Figure 6: Frequency of changes in the surface density of islands (A) and holes (B) as a function of total surface excess, at selected grafting densities. C, D, and E show examples of the types of events which may change the number of islands or holes in the images. In each case successive snapshots of the simulation are shown, separated in time by 400τ. Black regions represent polymer-free areas and white regions represent polymer covered areas. C shows the fusion of one pair of micelles (shaded blue) and the fission of another larger micelle into two (shaded pink) on a surface with $N\rho = 0.96\sigma^{-2}$ and $\Gamma_{\text{total}} = 1.23\sigma^{-2}$. D ($N\rho = 2.08\sigma^{-2}$ and $\Gamma_{\text{total}} = 2.65\sigma^{-2}$) shows the nucleation of a hole (shaded red), while E ($N\rho = 2.08\sigma^{-2}$ and $\Gamma_{\text{total}} = 2.48\sigma^{-2}$) shows the fission of a large hole into two smaller holes (shaded red).

may change the number of micelles – fusion of two smaller micelles into a larger and typically elongated micelle; and fission of such a larger micelle into two smaller micelles. Examples of these processes can be seen in Figure 6C, which shows two successive snapshots separated in time by 400τ. Two micelles on the left, shaded blue, fuse together, while one on the right, shaded pink, undergoes fission into two smaller micelles. In the pancake micelle regime the distance between micelles is only slightly greater than the chain separation, lowering the barrier to fusion between neighboring micelles.

When the total surface excess approaches the worm-like regime, approximately in the range $1.9\sigma^{-2} < \Gamma_{\text{total}} < 2.3\sigma^{-2}$, the frequency of changes rapidly falls towards zero as micelles cease to be present in significant numbers, as seen in Figure 6A. In the low grafting density case, when $N\rho = 0.82\sigma^{-2}$ (diamond shaped markers in Figure 6A), the frequency does not approach zero at high Γ_{total}. This is due to the sparse nature of the brush at this grafting density, and the high mobility of the chains in the presence of a relatively large amount of solvent – more than one solvent molecule for every monomer. The majority of the time a highly interconnected polymer layer is formed, however it is not uncommon for large discrete islands to briefly become disconnected from the network. This can be seen in Figures 3A and C which show that only a small number of islands are observed in this regime, with a wide spread of sizes.

We also see in Figure 6A that for a given Γ_{total}, the frequency of morphological changes is higher when the solvent content of the brush is greater (that is, when the grafting density is lower). Two possible reasons for this may include the fact that the addition of solvent should reduce the viscosity of the layer, making it more dynamic; and the formation of solvent bridges between micelles, which might act to reduce the energy barrier to micelle fusion by providing a lower energy path for chains to move out from the micelle nucleus in which they initially resided.

In Figure 6B we see the frequency of changes in the hole density. Again there are multiple ways in which the number of holes in the layer may change over time. As in the micelle case, fission and fusion of holes is observed, particularly near the point at which the number of holes is near a maximum. Two other processes are also observed – nucleation of new holes in polymer covered regions, and the collapse of existing holes. An example of hole nucleation can be seen shaded in red in Figure 6D, while fusion can be seen in Figure 6E.

Hole nucleation and collapse have no analogous process in the micelle regime. We could conceive of a process by which a micelle is destroyed by the sudden dispersion of its chains into the surrounding micelles. Alternatively an entirely new micelle might nucleate in the space between existing micelles by extracting chains from nearby aggregates. Such processes are never observed in our simulations, probably due to the low probability of a large number of chains spontaneously moving in such a coordinated manner, and the high energy barrier to moving all the chains involved out of their initial micelles.

As Γ_{total} increases in Figure 6B, the frequency of hole density changes initially increases as we move from the worm-like regime into the holey layer regime, until a maximum is reached near $\Gamma_{\text{total}} = 2.4\sigma^{-2}$. The frequency then decreases to a minimum near $\Gamma_{\text{total}} = 2.6\sigma^{-2}$, which corresponds to the point at which the number of holes per unit area is at a maximum, as seen in Figure 3B. As Γ_{total} is increased further the frequency increases to another local maximum near $\Gamma_{\text{total}} = 2.9\sigma^{-2}$. This second maximum occurs when Γ_{total} is slightly less than the critical Γ_{total} at which the transition between holey layer and homogeneous layer occurs, also seen in Figure 3B. Increasing Γ_{total} further results in the frequency rapidly decreasing towards zero as the homogeneous layer regime is approached at approximately $\Gamma_{\text{total}} = 3.0\sigma^{-2}$.

The local minimum in the frequency coincides with the point at which the number of holes is at a maximum. At this point there is little remaining space for new holes to nucleate, but also enough space between holes to act as barrier to hole fusion. At lower total surface excess, the size of the holes increases and smaller holes are able to fuse into larger holes, increasing the number of fusion and fission events. At higher total surface excess, more spaces exist between holes into which new holes may nucleate, although such a nucleation may reduce the local surface coverage too much, and therefore result in the later collapse of the new hole or another preexisting hole. The presence of two local maxima in the frequency therefore appears to be tied to the two different classes of dynamic processes – fusion and fission at low total surface excess, and nucleation and hole collapse at higher total surface excess. This stands in contrast to the micelle regime in Figure 6A, which has only one maximum due to the fact that fission and fusion are the only possible processes.

Application as tunable nano-patterns

The ability to tune the nano-pattern morphology by the adsorption of smaller molecules opens up the potential for application of the layers formed by constrained dewetting as functional surfaces. A polymer brush with a specific grafting density immersed in a pure poor solvent will forever be fixed in that particular pattern regime. If, however, a small amount of a good solvent could be introduced into the solvent-mixture, then the pattern characteristics could be controlled by varying the concentration of the good solvent and thus the solvent surface excess. If the surface was made with a contrast in the chemical properties of the substrate and polymer, then it may be possible to finely tune the overall functionality.

As an example, in a previous publication[18] we showed that patterns formed by constrained dewetting could potentially be used as a mixed-boundary condition surface, over which fluid flows at different rates over the polymer compared to the exposed substrate. Such surfaces have been shown to have applications as microfluidic mixers.[27] The introduction of a small amount of good solvent could allow the fraction of covered surface to be varied, varying the degree of mixing or even switching it off completely.

Conclusions

We have performed the first study of which we are aware on the effect of the adsorption of small amounts of a good solvent on the morphology and dynamics of the polymer nano-patterns formed during constrained dewetting. The key conclusions are as follows:

- In the case of the dry layer we found nano-patterns similar to those observed by previous studies. The features of these patterns would be on the order of 10 nm for polymer chains with length comparable to those simulated (24 monomer units) and a typical monomer size of a few angstroms. As solvent is removed from a swollen polymer brush, it passes through the same morphological regimes as those seen in dry brushes at different grafting densities – holey layer, worm-like layer, pancake and pinned micelles.

- In a polymer brush containing adsorbed good solvent, the pattern features changed to resemble that which would be expected for a higher grafting density. The morphology of the pattern formed is a function of the sum of the number of monomer units and adsorbed solvent atoms per unit area, which we have referred to as the total surface excess Γ_{total}. A pancake micelle layer can potentially be switched to a holey layer by adsorbing an appropriate concentration of good solvent. The grafting density plays a relatively minor role in determining the morphology at a given total surface excess.

- The solvent preferentially adsorbs within the polymer aggregates rather than on the bare substrate.

- The dynamics of formation and collapse of features within these patterns were analyzed for the first time. Pattern features change over time, with the rate at which features merge and separate – and in the case of holey layers, nucleate and collapse – depending on the grafting density and solvent content. Changes in pattern features become more frequent in proximity to the transition near the upper grafting density limit of the micelle regime, where micelle fusion and fission events become common. Peaks in the frequency of changes also occur at both ends of the holey layer regime, with hole fusion and fission events common at the lower grafting density limit, and nucleation and collapse events common near the transition to the homogeneous layer.

The approximate equivalence between free and bound molecules present in the polymer layer suggests the use of polymer brushes as a platform to fabricate tunable nano-patterned surfaces. The nano-pattern morphology formed by a polymer brush immersed in a poor solvent – perhaps in a microfluidic device – could be dynamically tuned by adding a small amount of good solvent into the system. The knowledge of the pattern dynamics we have described would be important for the application of the polymer brush patterns. For example, if these layers were employed in an application which required stable patterns, then the lower grafting density end of the pinned micelle regime might be the most appropriate.

Acknowledgement

C.N. and S.C.H. acknowledge the Australian Research Council for funding, and C.N. acknowledges The University of Sydney for funding. This work was supported by an award under the Merit Allocation Scheme on the NCI National Facility at the Australian National University.

Supporting Information Available

Details of image analysis methods, and video files showing the changes in polymer distribution during evaporation of solvent form the polymer brush.

This material is available free of charge via the Internet at `http://pubs.acs.org/`.

References

(1) de Gennes, P. G. *Adv. Colloid Interfac.* **1987**, *27*, 189–209.

(2) Zhou, F.; Huck, W. T. S. *Phys. Chem. Chem. Phys.* **2006**, *8*, 3815–3823.

(3) Ouyang, H.; Xia, Z.; Zhe, J. *Microfluid. Nanofluid.* **2010**, *9*, 915âĂŞ922.

(4) *Polymer Brushes: Synthesis, Characterisation, Applications*; Wiley-VCH: Weinheim, Germany, 2004.

(5) Barbey, R.; Lavanant, L.; Paripovic, D.; SchuÌĹwer, N.; Sugnaux, C.; Tugulu, S.; Klok, H.-A. *Chem. Rev.* **2009**, *109*, 5437–5527.

(6) Halperin, A. *J. Phys. France* **1988**, *49*, 547–550.

(7) Zhulina, E. B.; Borisov, O. V.; Pryamitsyn, V. A.; Birshtein, T. M. *Macromolecules* **1991**, *24*, 140–149.

(8) Huh, J.; Ahn, C.-H.; Jo, W. H.; Bright, J. N.; Williams, D. R. M. *Macromolecules* **2005**, *38*, 2974–2980.

(9) Pattanayek, S. K.; Pham, T. T.; Pereira, G. G. *J. Chem. Phys.* **2005**, *122*, 214908–14.

(10) Soga, K. G.; Hong, G.; Zuckermann, M. J. *EPL* **1995**, *29*, 531.

(11) Williams, D. *J. Phys. II France* **1993**, *3*, 1313–1318.

(12) Koutsos, V.; van der Vegte, E. W.; Hadziioannou, G. *Macromolecules* **1999**, *32*, 1233–1236.

(13) Zhao, W.; Krausch, G.; Rafailovich, M. H.; Sokolov, J. *Macromolecules* **1994**, *27*, 2933–2935.

(14) O'Shea, S. J.; Welland, M. E.; Rayment, T. *Langmuir* **1993**, *9*, 1826–1835.

(15) Yoon, B.; Huh, J.; Ito, H.; Frommer, J.; Sohn, B. H.; Kim, J. â.; Thomas, E. â.; Park, C.; Kim, H. C. *Adv. Mater.* **2007**, *19*, 3342–3348.

(16) Zhulina, E.; Singh, C.; Balazs, A. C. *J. Chem. Phys.* **1997**, *108*, 1175–1183.

(17) Yeung, C.; Balazs, A. C.; Jasnow, D. *Macromolecules* **1993**, *26*, 1914–1921.

(18) Lee, T.; Hendy, S. C.; Neto, C. *Macromolecules* **2012**, *45*, 6241–6252.

(19) Plimpton, S. J. *J. Comput. Phys.* **1995**, *117*, 1–19.

(20) Chatani, Y.; Shimane, Y.; Ijitsu, T.; Yukinari, T. *Polymer* **1993**, *34*, 1625 – 1629.

(21) Jeon, S.; Lee, J.; Andrade, J.; Gennes, P. D. *J. Colloid Interf. Sci.* **1991**, *142*, 149 – 158.

(22) Mooney, R. C. L. *J. Am. Chem. Soc.* **1941**, *63*, 2828–2832.

(23) Kremer, K.; Grest, G. S. *J. Chem. Phys.* **1990**, *92*, 5057–5086.

(24) Hünenberger, P. H. In *Advanced Computer Simulation*; Holm, C., Kremer, K., Eds.; Adv. Polym. Sci.; Springer Berlin Heidelberg, 2005; Vol. 173; pp 105–149.

(25) Seul, M.; O'Gorman, L.; Sammon, M. J. *Practical algorithms for image analysis: descriptions, examples, and code*; Cambridge University Press: Cambridge, 2000.

(26) Mcnaught, A. D.; Wilkinson, A. *IUPAC. Compendium of Chemical Terminology, 2nd ed. (the "Gold Book")*; Wiley Blackwell; 2nd Revised edition.

(27) Hendy, S. C.; Jasperse, M.; Burnell, J. *Phys. Rev. E* **2005**, *72*, 016303.

Table of Contents Graphic

Tunable Nano-Patterns via the Constrained Dewetting of Polymer Brushes

Thomas Lee, Shaun C. Hendy, and Chiara Neto